

Effect of thickness and microstructure of TiO₂ shell on photocatalytic performance of magnetic separable Fe₃O₄/SiO₂/mTiO₂ core-shell composites

Dandan Wang^{1,2,3}, Jinghai Yang^{*,3}, Xiuyan Li^{**3}, Jian Wang³, Hongju Zhai⁴, Jihui Lang³, and Hang Song¹

¹ Changchun Institute of Optics, Fine Mechanics and Physics, Chinese Academy of Sciences, Changchun 130033, P.R. China

² University of Chinese Academy of Sciences, Beijing 100049, P.R. China

³ Key Laboratory of Functional Materials Physics and Chemistry of the Ministry of Education, Jilin Normal University, Siping 136000, P.R. China

⁴ Key Laboratory of Preparation and Applications of Environmental Friendly Materials of the Ministry of Education, Jilin Normal University, Siping 136000, Jilin, P.R. China

Received 5 September 2016, revised 2 February 2017, accepted 3 February 2017

Published online 27 February 2017

Keywords core-shell structures, magnetic separation, mesoporous materials, oxides, photocatalysis, TiO₂

* Corresponding author: email jhyang1@jlnu.edu.cn, Phone: +86 434 3294566, Fax: +86 434 3294566

** email lixiuyan@jlnu.edu.cn, Phone: +86 434 3294566, Fax: +86 434 3294566.

Here, unique Fe₃O₄/SiO₂/mTiO₂ (FST) composites were fabricated, which are composed of a Fe₃O₄ core with a strong response to magnetic field, an intermediate SiO₂ layer as an electronic barrier, and an outer mesoporous TiO₂ (mTiO₂) as the active layer for degradation of organic contaminants. The distinctive approach involved TiO₂ shell coating on the surface of Fe₃O₄/SiO₂ (FS) particle using a sol-gel method, followed by the crystallization and mesopore-formation of TiO₂ through solvothermal treatment. By changing the dosage of tetrabutyl titanate (TBOT), the thickness and microstructure of TiO₂ layer

were regulated. Among all as-prepared FST composites, the FST composite that was prepared with 0.6 ml TBOT (FST-0.6) possessed a good microstructure and a large specific surface area, and exhibited superior photocatalytic activity toward the degradation of methylene blue (MB) solution. Moreover, recovered FST-0.6 composite with the help of an appropriate magnetic field maintained the activity without significant decline during multiple photocatalytic tests. Accordingly, a rational mechanism was proposed to explain why the FST-0.6 composite showed excellent photocatalytic performance.

© 2017 WILEY-VCH Verlag GmbH & Co. KGaA, Weinheim

1 Introduction During the past few decades, considerable efforts have been devoted to purging synthetic organic pollutants out of the environment by using photocatalytic methods. Among various types of photocatalysis, semiconductor photocatalysis has been recognized as the “green chemistry” technology due to its low toxicity and ideal products of CO₂ and H₂O [1, 2]. TiO₂ material has been proven to be an effective semiconductor photocatalyst due to its excellent degradation capacity, low cost and high chemical stability against both photo and chemical corrosion [3–5]. The degradation mechanism of TiO₂ photocatalysts is as follows: when TiO₂ are exposed to

UV light, electrons in the uppermost valence band jump to the conduction band and create electron-hole pairs. The photo-generated electrons and holes can induce the formation of reactive oxygen species (ROS: OH·, HO₂·, H₂O₂, ¹O₂) that are directly involved in the photocatalytic conversion of organic pollutants into green products [6, 7]. Unfortunately, the recovery and separation of TiO₂ ordinarily require complex centrifugation or filtration processes, which would result in high costs, thus, restricting the practical application of pure TiO₂ in water treatment. Therefore, the efficient recovery of nanoscale TiO₂ from treated water is a challenge for practical applications.

Based on potential applications of magnetic materials (such as magnetite, barium ferrite) in catalysis, selective separation, chemical and biologic sensors, composites including magnetic core and functional shell have been extensively investigated in recent years [8–11]. Magnetic Fe₃O₄ have been considered as a suitable support due to its outstanding superparamagnetism, flexible surface functionalization, and favorable dispersity [12–16]. Xin et al. have synthesized magnetic separable Fe₃O₄@TiO₂ core-shell composite, which has confirmed that the negligible remanent magnetism of Fe₃O₄ can avoid forming magnetic aggregates in a photocatalytic reaction. Meanwhile, Fe₃O₄ core with superparamagnetism can provide a convenient approach for recycling the photocatalyst from treated water by applying an external magnetic field [17]. However, the process of photocatalysis usually destroys the magnetic properties of the Fe₃O₄ supporter, especially under acidic conditions [18, 19]. At the same time, a direct contact between Fe₃O₄ and TiO₂ typically brings about an unfavorable heterojunction, which accelerates the recombination of the electron-hole pairs and weakens the photocatalytic activity of titanium-based catalysts [20–22]. To maintain the photocatalytic activity of TiO₂ and protect the magnetic properties of Fe₃O₄ carrier, choosing a stable material, as an intermediate layer between Fe₃O₄ carrier and TiO₂ photocatalyst, is necessary.

At present, most researchers employ the well-known sol-gel method to prepare composite titanium-based catalysts. But the obtained TiO₂ is normally amorphous and has no photocatalytic activity. Accordingly, heat treatment (500–800 °C) is generally required to induce crystallization and photocatalytic activity of hydrous TiO₂. Unfortunately, high-temperature annealing easily induces a transition of Fe₃O₄ to antiferromagnetic γ -Fe₂O₃ phase [12, 23, 24]. Thus, in order to protect the magnetic properties of Fe₃O₄, finding a convenient method to prepare crystalline TiO₂ is urgently needed.

To improve the practicality of TiO₂ material in photocatalytic field, in this work, we successfully fabricated unique FST core-shell composites including a Fe₃O₄ microsphere as the core, a SiO₂ layer as the protective layer in the middle and an outer TiO₂ layer. The TiO₂ layer was prepared by combining the sol-gel process and solvothermal method without high-temperature calcinations, which had a porous structure and high crystallinity. The thickness and microstructure of TiO₂ layer was adjusted by changing the dosage of TBOT. Among all as-prepared FST composites, the well-designed FST-0.6 composite exhibited superior photocatalytic activity. In addition, the magnetically recovered FST-0.6 composite had a steady activity after 6 times of running the photocatalytic test. Hence, our work provides new insights into the control of the microstructure and enhancement of the photocatalytic activity of magnetic photocatalyst, and should be of great interest for photocatalysis, separation technology, and nanotechnology.

2 Experimental

2.1 Materials

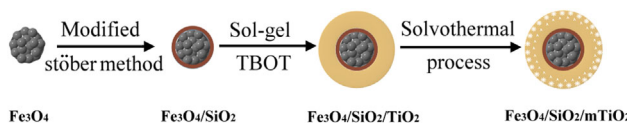
Iron(III) chloride hexahydrate (FeCl₃ · 6H₂O), trisodium citrate, sodium acetate (NaAc), tetraethyl orthosilicate (TEOS), aqueous ammonia solution (25 wt.%), tetrabutyl titanate (TBOT), acetonitrile, ethanol, and ethylene glycol of analytical grade were purchased from Sinopharm Chemical Reagent Co. Ltd. Deionized water (resistivity >18.0 MΩ cm) was used throughout the study. All chemicals were used as is without additional purification.

2.2 Preparation of magnetic photocatalysts

The synthesis of core-shell FST composites is illustrated in Scheme 1. First, Fe₃O₄ (F) sample was prepared via the solvothermal method [25]. FeCl₃ · 6H₂O (2.16 g) was dissolved in ethylene glycol (40 ml) under magnetic stirring. Subsequently, NaAc (3.6 g) and trisodium citrate (1.0 g) were added to the formed clear yellow solution. The mixture was stirred until the reactants were fully dissolved. Then, the obtained homogeneous dispersion was transferred to a 100 ml teflon-lined stainless-steel autoclave and heated at 200 °C for 10 h. The black powders were collected by an applied magnetic field, followed by rinsing several times with deionized water and ethanol. The product was dried in vacuum at 60 °C for 6 h.

SiO₂ was coated on F core using the modified Stöber method [26]. Typically, the obtained F sample (0.5 g) was dispersed in a mixed solution of deionized water (50 ml), ethanol (150 ml), and ammonia aqueous solution (25 wt.%, 2.0 ml) under ultrasonication for 1 h. Subsequently, TEOS (0.8 ml) was added dropwise to this dispersion. After being stirred for 2 h, the product was separated using a magnet, washed with deionized water, and then dried at 60 °C for further use.

The preparation of TiO₂ shell includes two steps. First, the as-prepared FS product (0.05 g) was dispersed in a mixture of ethanol (90 ml), acetonitrile (30 ml), and ammonia aqueous solution (25 wt.%, 0.5 ml) under vigorous stirring. Then, a certain amount of TBOT was added to this mixture. TiO₂ shell was prepared on the surface of FS after being stirred at ambient temperature for 1.5 h. This TiO₂ shell, however, was amorphous and had no photoactivity [17]. Secondly, the obtained FST powders were dispersed in ethanol (40 ml) and mixed with deionized water (20 ml). Then, the mixture was transferred into a 100 ml teflon-lined stainless-steel autoclave for solvothermal treatment at 160 °C for 20 h, during which TiO₂ crystallized. The final product was collected by an



Scheme 1 Illustration of synthetic procedure for FST core-shell composites.

external magnetic field, washed with ethanol and dried at 60 °C for 6 h.

The thickness and microstructure of TiO₂ shell were tuned by adjusting the dosage of TBOT (0.3, 0.6, and 0.9 ml TBOT, respectively). FST-0.3, FST-0.6, and FST-0.9 were used to represent different FST products in this article, respectively.

2.3 Characterization The morphology and structure of the as-synthesized samples were examined by using a field emission scanning electron microscopy (FESEM, JEOL 7800F) and a transmission electron microscopy (TEM, FEI Tenai G² F20). The crystal structures of all as-prepared samples were analyzed by a D/max-2500 copper rotating-anode X-ray powder diffraction with Cu K_α radiation ($\lambda = 1.5406 \text{ \AA}$) at 40 kV and 200 mA. X-ray photoelectron spectra (XPS) were recorded on a Thermo Scientific ESCALAB 250Xi A1440 system. Nitrogen sorption isotherms were measured by using a Nova 1000 analyzer, and the pore-size distribution was derived from the desorption branch of the nitrogen adsorption–desorption isotherms using the Barrett–Joyner–Halenda (BJH) method. The magnetic properties were assessed by using a vibrating sample magnetometer (VSM, Lake Shore 7407) at 298 K.

The photoelectrochemical measurements were performed by using a computer-controlled electrochemical work station (CHI-660C Instruments, China). A conventional three electrode cell was used, which composed of the as-prepared powders coated on the indium–tin oxide glass (ITO) as the working electrode, a saturated calomel electrode (SCE) as a reference, and platinum as a counter electrode. The supporting electrolyte was 0.5 M Na₂SO₄ solution. A 500 W xenon lamp was used as a light source. Time-dependent photoresponse tests were carried out by measuring the photocurrent under chopped light irradiation (light/dark cycles of 20 s) at an applied potential of -0.5 V .

2.4 Photocatalytic activity measurement The photocatalytic activity of the as-prepared FST composites was measured by the degradation of MB solution (10 mg l⁻¹). In a typical experiment, FST (0.05 g) sample was dispersed in 100 ml of MB solution. To achieve an adsorption–desorption equilibrium, the suspension was continuously stirred in the dark for 20 min. A 250 W high-pressure Hg lamp with a main radiation wavelength of 365 nm was used as the UV radiation source. The average light intensity was estimated to be 22.11 mW cm⁻². At given intervals of illumination, the mixed suspension was sampled and FST composites were removed by a magnet. The supernatant liquid was determined by recording the maximum absorbance of MB at 652 nm with a UV-vis spectrophotometer (UV-5800PC, Shanghai Metash Instruments Co., Ltd.).

3 Result and discussion

3.1 Characterization of the as-prepared composites

Figure 1a and b presents SEM and TEM

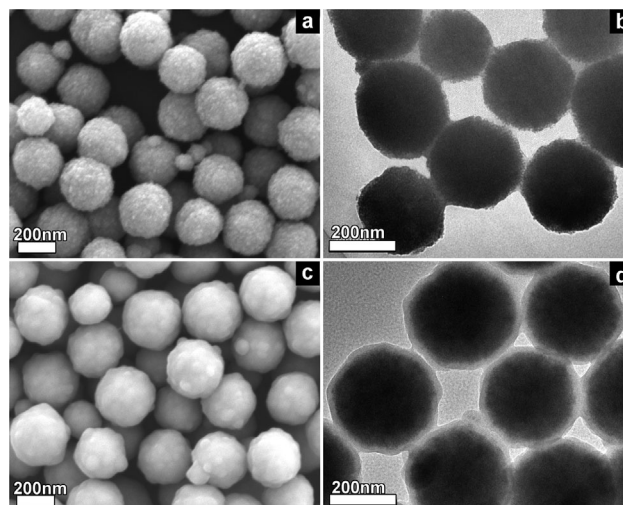


Figure 1 SEM and TEM images of (a, b) F and (c, d) FS samples.

images of F sample, respectively. The prepared F particles have a rough surface and the average diameter is about 260 nm. Meanwhile, F particles have good dispersity, which can be attributed to citrate stabilizer covered on the surface of F particles in the process of synthesis [27]. After coating the SiO₂, the product retains the morphological properties of F particles as shown in Fig. 1c. Compared to the F particle, the FS particle is larger and has a smooth surface. It can be seen from Fig. 1d that FS particle possesses a core-shell structure and SiO₂ shell shows a gray color with a mean thickness of about 20 nm.

Figure 2 shows SEM and TEM images of the three FST samples, respectively, and the physical properties of FST composites are summarized in Table 1. Here, TiO₂ easily grows on FS particles because Si–OH groups overspread on

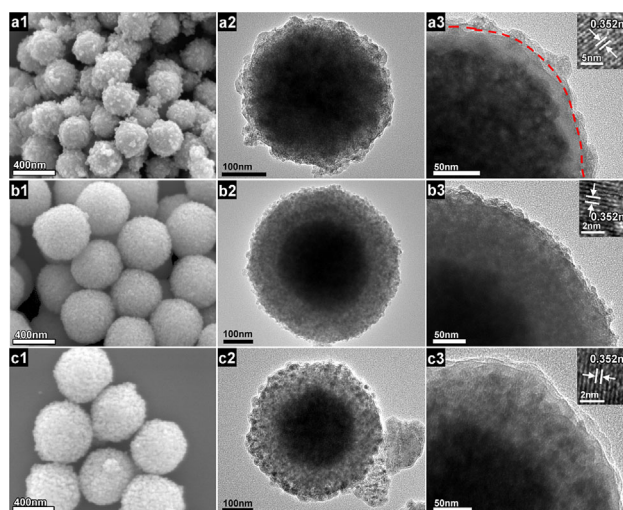


Figure 2 SEM and TEM images of (a1–3) FST-0.3, (b1–3) FST-0.6, and (c1–3) FST-0.9 composites; illustrations are the corresponding HTEM images.

Table 1 The physical properties of FST core-shell composites used in this work.

sample	size (nm)	thickness of TiO ₂ layer (nm)	MS (emu g ⁻¹)	pore diameter (nm)	SBET (m ² g ⁻¹)	degradation ratio (%)
FST-0.3	320	10	40.22	–	18.33	35.1
FST-0.6	520	100	31.23	15	101.21	90
FST-0.9	520	100	24.24	56	68.68	73.1

the surface of FS, providing available reactive site for the coating of TiO₂ [28]. When 0.3 ml TBOT is used to produce the FST composite, the as-prepared TiO₂ layer is uneven (Fig. 2a1 and a2). As shown in Fig. 2a3, the FST-0.3 composite has a clear core-shell microstructure including an F core, a SiO₂ middle layer and an outer TiO₂ layer. As shown in Fig. 2a3, it is easy to distinguish the TiO₂ layer with a thickness of around 10 nm from the SiO₂ layer using a red dotted line. When the dosage of TBOT is increased to 0.6 ml, the TiO₂ shell with a thickness of about 100 nm is well wrapped on the surface of the FS particle (Fig. 2b1 and b2). As shown in Fig. 2b3, the SiO₂ intermediate layer compared with the TiO₂ shell is so thin that it is not seen in FST-0.6 core-shell composites (FST-0.9 composite shows the same). When 0.9 ml of TBOT is added, the thickness of the TiO₂ shell is still about 100 nm (Fig. 2c1 and c2). But the microstructure of the TiO₂ layer shows some differences between the FST-0.6 and FST-0.9 composites. As presented in Fig. 2c2, larger TiO₂ particles constitute the TiO₂ layer of the FST-0.9 composite, and some isolated TiO₂ clusters scatter around the FST-0.9 composite that do not exist in the FST-0.6 composite. The insets in Fig. 2 are the corresponding HTEM images, that show a lattice fringe with a spacing of 0.351 nm, which is in agreement with the (101) plane of anatase TiO₂ (JCPDS card No. 21-1272). It clearly shows that when TiO₂ was deposited onto the surface of the SiO₂ middle layer, the obtained TiO₂ is pure anatase and not mixed phases of TiO₂ and SiO₂.

The surface energy is lower for the heterogeneous nucleation than that for the homogeneous nucleation, which can help to understand the above results [29]. At a lower concentration of TBOT (0.3 ml), heterogeneous nucleation of TiO₂ significantly occurs on the surface of FS particles. When the dosage of TBOT is slightly increased (0.6 ml), both hydrolysis and condensation of TBOT are promoted. Meanwhile, the reaction kinetics is overwhelmingly strengthened and substantial supplies of titanium precursor make the TiO₂ layer grow rapidly in thickness. However, when higher content of TBOT is added (0.9 ml), the concentration of the titania precursor exceeds the critical supersaturation for a homogeneous nucleation. Therefore, the thickness of the TiO₂ layer does not further increase while the large TiO₂ particles, which coat the surface FS particles, are formed [17]. And some scattered TiO₂ particles exist around FST-0.9 particles (Fig. 2c3). It can be concluded that a heterogeneous coating is dominating at lower concentration of TBOT, while homogeneous nucleation and growth occur at higher concentration.

All as-prepared products were examined by XRD to confirm crystal structure and compositional variation. The characteristic diffraction peaks, which are marked as (220), (311), (400), (422), (511), (440), and (533) in Fig. 3, can be indexed to the typical cubic phase of Fe₃O₄ (JCPDS card No. 19-0629). These sharp and intense peaks indicate that F particles have fine crystallized structure. A broad and weak peak centered at about 22° in Fig. 3b indicates that amorphous SiO₂ has been coated on the surface of F particles. Figure 3c shows the XRD pattern of FST-0.3 composite before the solvothermal treatment (FST-0.3b), which is almost the same as that of the FS sample. There are no characteristic peaks of TiO₂ in Fig. 3c, indicating that this TiO₂ is amorphous. After the process of solvothermal treatment, Fig. 3d, e, and f exhibit some well-defined peaks that are assigned to the (101), (004), (200), and (105) planes of the pure anatase phase (JCPDS card No. 21-1272), indicative of the high crystallinity of these TiO₂ layers. The well crystallinity is consistent with the result of HTEM images in Fig. 2. This also indicates that amorphous TiO₂ shell crystallizes in solvothermal treatment. In addition, by comparing all XRD diffraction patterns, it can be found that the coating of SiO₂ and TiO₂ weakens the peak intensity of F but does not affect its phase structure. Judging from the XRD and TEM results, FST composites including the F core, the SiO₂ middle layer, and the TiO₂ layer have been

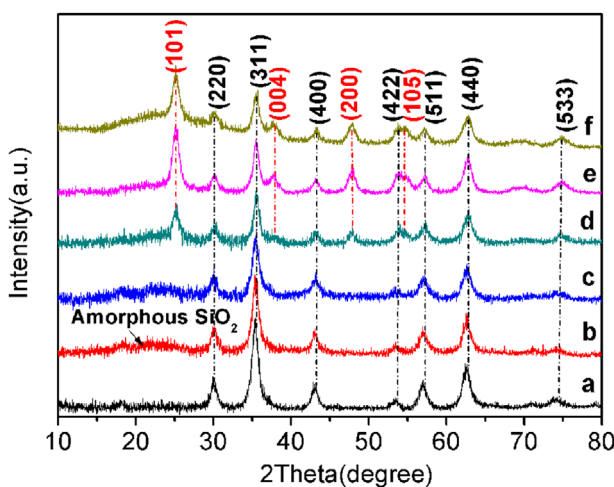


Figure 3 Powder XRD patterns of (a) F, (b) FS, (c) FST-0.3b (d–f) FST-0.3, FST-0.6, and FST-0.9 composites after solvothermal treatment, respectively.

successfully fabricated by the sol–gel process and solvo-thermal technology.

XPS analytical technique was used to illustrate the surface composition and bonding environment of all as-prepared samples. XPS fully scanned spectra of three FST composites are shown in Fig. 4a indicating that these FST composites contain O, Si, Ti, and C (remained from the adventitious carbon-based contaminant). XPS analysis is a highly surface-specific technique which can only reach ~ 10 nm depth of the sample [30]. And the F core is too far away from the particle surface after coating SiO_2 and TiO_2 . As a result, the signal binding energy of $\text{Fe}2p_{1/2}$ at ~ 710.7 eV is not found in the high-resolution XPS spectra of FS and FST-0.3 composites, which only exists in the high-resolution XPS spectra of F sample, as shown in Fig. 4b. This result signifies that SiO_2 is well coated on the surface of F cores. The high-resolution XPS spectra of $\text{Ti}2p$ of three FST composites are presented in Fig. 4c. The characteristic peaks at 458.4 and 464.4 eV are assigned to $\text{Ti}2p_{3/2}$ and $\text{Ti}2p_{1/2}$, respectively, suggesting that the valence of Ti is four, according to the National Institute of Standards and Technology (NIST) XPS database.

The porous structure and the specific surface area of FST core-shell composites were studied by N_2 adsorption–desorption analysis. Figure 5 presents the isotherm plots of three FST composites, respectively. According to the International Union of Pure and Applied Chemistry (IUPAC), the isotherm plot with a hysteresis loop is type IV pattern which confirms porous characteristic of FST-0.6

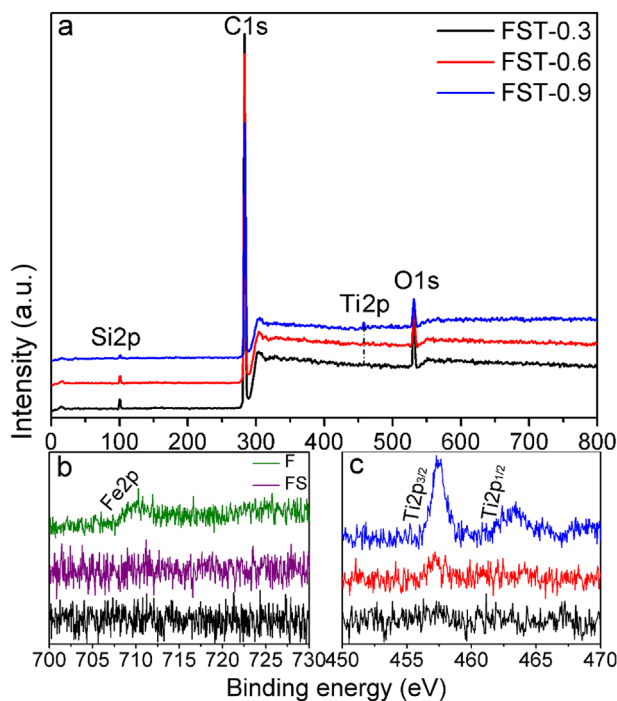


Figure 4 (a) XPS fully scanned spectra for three FST composites; (b) XPS spectra of $\text{Fe}2p$ for F, FS, and FST-0.3 samples, respectively; (c) XPS spectra of $\text{Ti}2p$ for three FST composites.

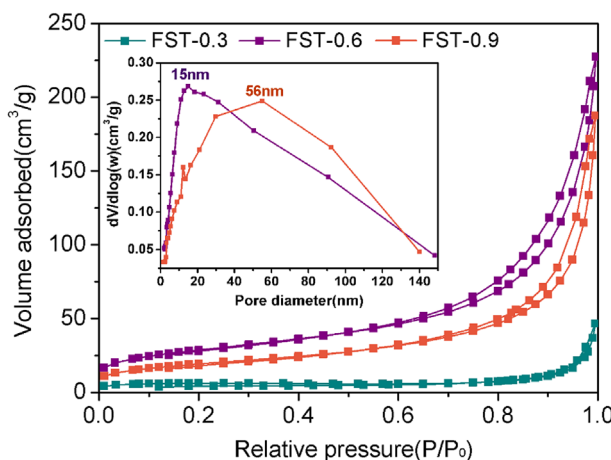


Figure 5 N_2 adsorption–desorption isotherms of three FST composites; the insets are corresponding pore size distribution curves of FST-0.6 and FST-0.9 composites.

and FST-0.9 composites. However, there is no adsorption–desorption hysteresis loop in the isotherm plot of FST-0.3 composite, indicating that FST-0.3 is not a mesoporous material. The corresponding pore-size distribution is evaluated by using the BJH model. The inset in Fig. 5 shows the pore size distribution curve of FST-0.6 and FST-0.9 composites, respectively. The pore size distribution curve of FST-0.6 composite contains a fractional micropore (< 2.0 nm), a mesopore (2.0–50.0 nm) centered at 15 nm and a macropore (> 50.0 nm) with a maximum pore diameter of about 150 nm. A rational hypothesis is proposed for this pore size distribution curve: the micropore can be related to the interlayer of SiO_2 [31]. The mesopore is ascribed to two different pores in the TiO_2 shell, including smaller mesopore results from primary TiO_2 nanocrystals stacking with each other, and the larger mesopore forms between the TiO_2 particles on the edge of the TiO_2 shell [32, 33]. The macropores are produced by stacked FST-0.6 composite. The pore sizes of FST-0.9 composite are mainly distributed in the macropore. This result can be attributed to its microstructure of the TiO_2 shell, which is primarily composed of larger TiO_2 particles.

In addition, compared to the FST-0.3 composite ($18.33 \text{ m}^2 \text{ g}^{-1}$) and P25 ($50 \pm 15 \text{ m}^2 \text{ g}^{-1}$), the as-prepared FST-0.6 and FST-0.9 composites have higher specific surface area of about 101.21 and $68.68 \text{ m}^2 \text{ g}^{-1}$, respectively. This result indicates that the porous TiO_2 shell in FST-0.6 and FST-0.9 composites brings about an increase in the surface area.

3.2 Photocatalytic and photoelectrochemical properties of as-prepared composites

MB dye solution was used as the model to evaluate the photocatalytic activities of all as-prepared FST samples. Figure 6 shows photocatalytic activities of different FST composites in comparison with commercial Degussa P25. After a 90 min photocatalytic degradation under UV radiation, the blank experiment (without photocatalyst) demonstrates that the

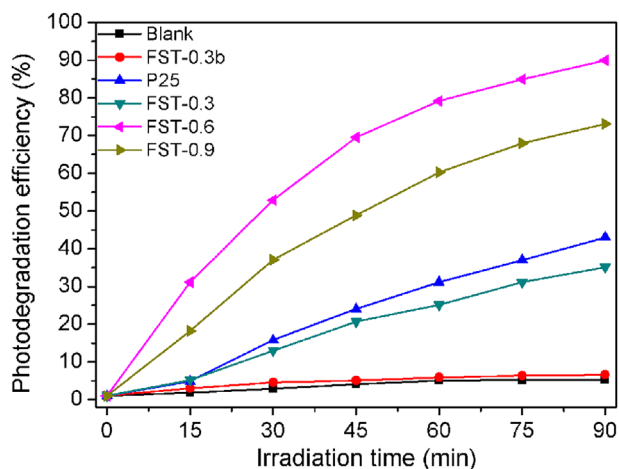
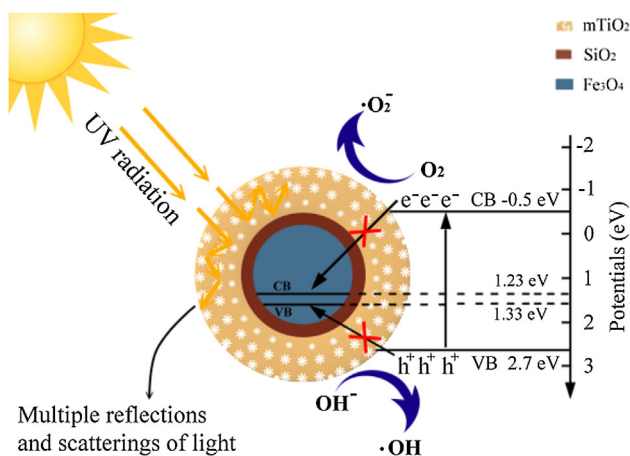


Figure 6 The photodegradation efficiency of MB by all as-prepared FST samples and P25.

photolysis of the MB solution is slow and FST-0.3b has almost no photocatalytic activity because its TiO₂ layer is amorphous. The decomposition rates of MB for FST-0.3, FST-0.6, FST-0.9, and P25 are 35.1%, 90.0%, 73.1%, and 42.9%, respectively.

N₂ adsorption analysis and TEM analysis results of the different FST composites can help to understand the differences in photocatalytic properties of the different samples. N₂ adsorption analysis states that the size of a specific surface area for different samples follows the sequence: FST-0.6 > FST-0.9 > P25 > FST-0.3. This order is in agreement with their photocatalytic activity. The larger specific surface area is convenient for the contact between the photocatalyst and the MB molecules, and possesses more exposed active sites for photocatalytic degradation. This is the main reason for the lowest activity of FST-0.3 composite. When FST composites are exposed to UV light, the transfer of the photogenerated electrons in the valence band and holes in the conduction band of TiO₂ to F core, can be completely inhibited by introducing a wide band gap SiO₂ layer, as shown in Scheme 2 [31]. The photo-induced electrons and holes from TiO₂ can react directly with the surrounding species (O₂ and ⁻OH), and produce ROS that are directly involved in the photocatalytic reaction. Therefore, the SiO₂ layer prevents the F core from becoming a recombination center of electrons and holes. Meanwhile, as presented in Scheme 2, multiple reflections and scatterings of the radiant light within the interior cavity can expand the propagation of light waves [34–36]. The utilization ratio to radiation light is improved for the mesoporous characteristic of FST-0.6 and FST-0.9 composites. Therefore, it is not difficult to understand why FST-0.6 and FST-0.9 composites exhibit superior photocatalytic activity to that of other samples.

Compared to FST-0.9 composite, FST-0.6 shows a much better photocatalytic activity. In addition to a larger specific surface, this can also be attributed to the uniform TiO₂ nanocrystals in FST-0.6 composite as shown in Fig. 2b1–b3. Small TiO₂ nanocrystals can give rise to the quantum confinement effects that benefit to the photogenerated carriers



Scheme 2 Schematic representation of proposed photocatalytic mechanism for FST composites.

separation [37–39]. The photocurrent spectra are shown in Fig. 7. A much higher photocurrent of the FST-0.6 composite than that of FST-0.3 and FST-0.9 indicates that the photogenerated electron–hole separation for the FST-0.6 samples has been improved. Therefore, FST-0.6 composite with the well-designed microstructure exhibits the best photocatalytic performance among all tested samples.

3.3 Magnetic properties and reusability of as-prepared composites

The magnetic properties of all as-obtained samples were characterized by a vibrating sample magnetometer. As shown in Fig. 8a, these hysteresis loops present a steep slope and have no remanence and coercivity, indicating that all samples have superparamagnetic behavior at room temperature. The magnetic saturation value (M_s) of F sample is 44.27 emu g⁻¹ and after coating the SiO₂ shell, the M_s value for FS sample is reduced to 42.91 emu g⁻¹. The M_s values of FST composites further decreased, and are 40.22,

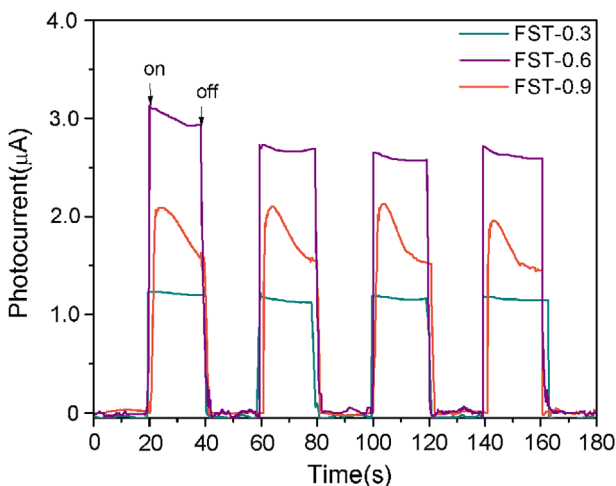


Figure 7 Photocurrent response of the as-prepared FST samples under UV light irradiation.

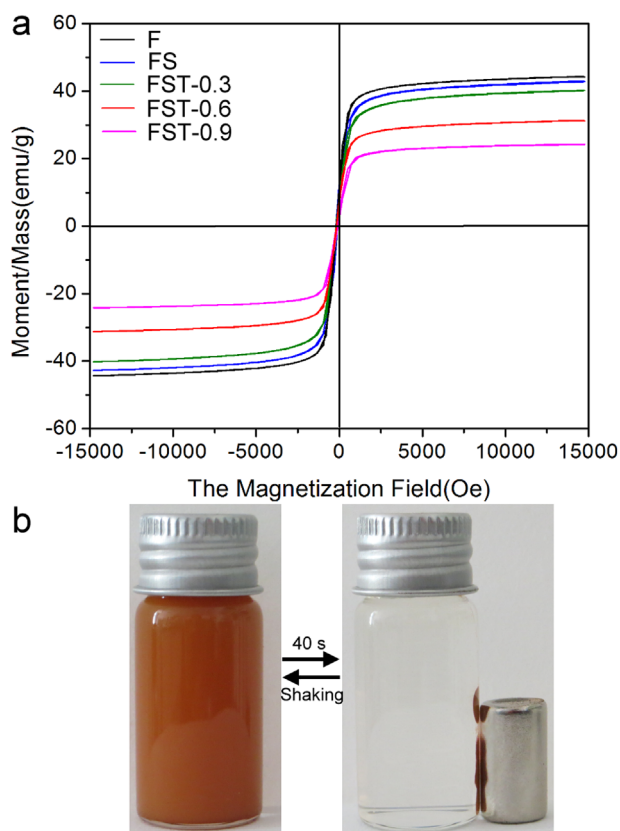


Figure 8 (a) The magnetic curves of F, FS, and different FST samples; (b) the separation-redispersion process of FST-0.9 composite in solution by using a magnet.

31.23, and 24.24 emu g^{-1} for FST-0.3, FST-0.6, FST-0.9 composites, respectively. The decrease of M_s values is consistent with the F content in unit weight composites. Figure 8b shows FST-0.9 composite gathered by using a magnet within only 40 s, and then re-dispersed into the solution with a slight shake after removing the magnetic field. Thus, when FST composites are aggregated with the help of a magnet, the liquid can be discarded and the FST photocatalyst recovered. It was concluded that the superparamagnetism of FST composites facilitates the recycling of FST photocatalyst by using an external magnetic field.

As shown in Fig. 9a, the catalytic stability of three FST composites was investigated by monitoring the decomposition rate of MB during multiple photocatalytic tests. Compared to other samples, FST-0.6 composite exhibited a relatively stable photocatalytic activity, which is attributed to the excellent structure of the FST-0.6 composite. As shown in Fig. 9b, the TEM image of FST-0.6 composite after multiple photocatalytic tests indicates that it has a steady structure. The stable microstructure can minimize the loss of TiO_2 particles in photocatalytic processes. In addition, three FST composites are separated from MB solution by using a magnet after each test, showing that the as-prepared FST composites also have a good magnetic stability.

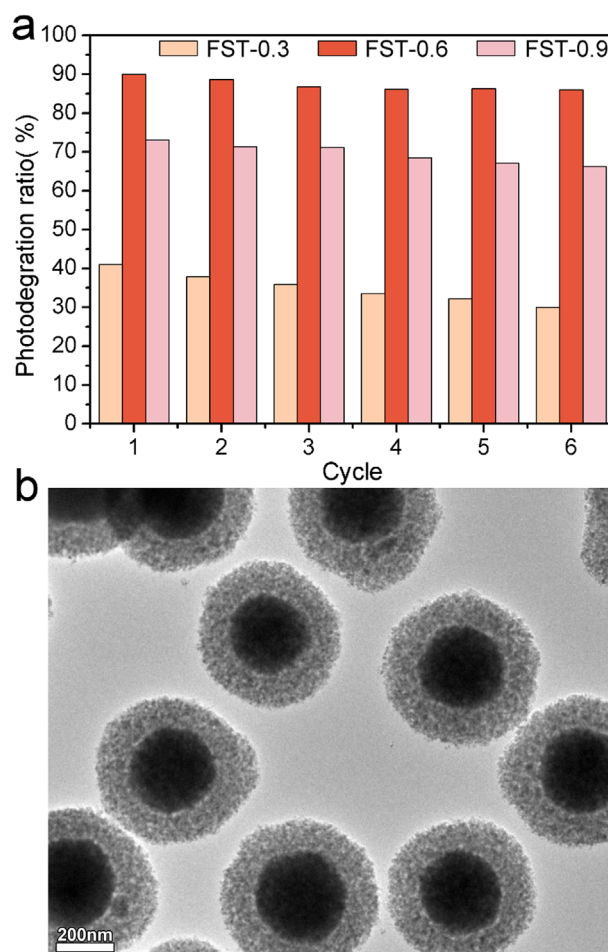


Figure 9 (a) Six cycles of the photocatalytic degradation of MB in the presence of different FST composites; (b) TEM image of FST-0.6 composite after repeating the photocatalytic tests for 6 times.

4 Conclusions Here, we successfully synthesized magnetic core-shell $\text{Fe}_3\text{O}_4/\text{SiO}_2/\text{mTiO}_2$ composites. The microstructure of TiO_2 layer was finely tuned during the preparation. The crystallization of TiO_2 was achieved by solvothermal treatment, and the dosage of TBOT significantly affected the thickness and the porous structure of TiO_2 . The results showed that the $\text{Fe}_3\text{O}_4/\text{SiO}_2/\text{mTiO}_2$ product prepared with a 0.6 ml tetrabutyl titanate (FST-0.6) had a superior microstructure, including a large specific surface area and a good mesoporous structure. Moreover, based on the synergy of different components, FST-0.6 sample exhibited excellent photocatalytic activity, fine magnetic properties, and chemical stability during multiple photocatalytic processes. Therefore, FST-0.6 core-shell composite can serve as an efficient and recyclable photocatalyst, which has promising applications in environmental treatment.

Acknowledgements This work is supported by the National Programs for High Technology Research and Development of China (863) (Item No. 2013AA032202), National Natural Science Foundation of China (Grant Nos. 61378085, 51479220,

61308095, and 51608226), Program for the development of Science and Technology of Jilin province (Item No. 20130102004JC, 201215222, and 20140101205JC), Program for New Century Excellent Talents in University (No. NCET-13-0824).

References

- [1] Z. Zhao, Z. C. Sun, H. F. Zhao, M. Zheng, P. Du, J. L. Zhao, and H. Y. Fan, *J. Mater. Chem.* **22**, 21965 (2012).
- [2] Q. Xiang, K. Lv, and J. Yu, *Appl. Catal. B Environ.* **96**, 557 (2010).
- [3] W. K. Jo and T. S. Natarajan, *Chem. Eng. J.* **281**, 549 (2015).
- [4] S. Liu, J. Yu, and W. Wang, *Phys. Chem. Chem. Phys.* **12**, 12308 (2010).
- [5] U. T. Pawar, S. A. Pawar, J. H. Kim, and P. S. Patil, *Ceram. Int.* **42**, 8038 (2016).
- [6] J. Yu, G. Wang, and B. Cheng, *J. Phys. Chem. Solids* **71**, 523 (2010).
- [7] J. Yu, Q. Xiang, and M. Zhou, *Appl. Catal. B Environ.* **90**, 595 (2009).
- [8] W. Wu, X. H. Xiao, S. F. Zhang, F. Ren, and C. H. Jiang, *Nanoscale Res. Lett.* **6**, 533 (2011).
- [9] I. Akin, G. Arslan, A. Tor, M. Ersoz, and Y. Cengelolu, *J. Hazard. Mater.* **235–236**, 62 (2012).
- [10] B. Cui, H. Peng, H. Xia, X. Guo, and H. Guo, *Sep. Purif. Technol.* **103**, 251 (2013).
- [11] Y. Deng, D. Qi, C. Deng, X. Zhang, and D. Zhao, *J. Am. Chem. Soc.* **130**, 28 (2008).
- [12] J. Yang, H. H. Chen, J. H. Gao, T. T. Yan, F. Y. Zhou, S. H. Cui, and W. T. Bi, *Mater. Lett.* **164**, 183 (2016).
- [13] C. F. Zhang, L. G. Qiu, F. Ke, Y. J. Zhu, Y. P. Yuan, G. S. Xu, and X. Jiang, *J. Mater. Chem. A* **1**, 14329 (2013).
- [14] M. V. Dozzia, S. Marzortia, M. Longhia, M. Codurib, L. Artigliac, and E. Sellia, *Appl. Catal. B Environ.* **186**, 157 (2016).
- [15] L. L. Tan, W. J. Ong, S. P. Chaia, B. T. Goh, and A. R. Mohamed, *Appl. Catal. B Environ.* **179**, 160 (2015).
- [16] X. X. Yu, J. G. Yu, B. Cheng, and M. Jaroniec, *J. Phys. Chem. C* **113**, 17527 (2009).
- [17] T. Xin, M. Ma, H. Zhang, J. Gu, S. Wang, M. Liu, and Q. Zhang, *Appl. Surf. Sci.* **288**, 51 (2014).
- [18] P. M. Rao and X. Zheng, *J. Am. Chem. Soc.* **11**, 2390 (2011).
- [19] V. Tyrpekl, J. P. Vejpravová, A. G. Roca, N. Murafa, L. Szatmary, and D. Nižňanský, *Appl. Surf. Sci.* **257**, 4844 (2011).
- [20] C. X. Wang, L. W. Yin, L. Y. Zhang, L. Kang, X. F. Wang, and R. Gao, *J. Phys. Chem. C* **113**, 4008 (2009).
- [21] D. Beydoun, R. Amal, G. K. C. Low, and S. McEvoy, *J. Phys. Chem. B* **104**, 4387 (2000).
- [22] S. Abramson, L. Srithammavanh, J. M. Siaugue, O. Horner, X. Xu, and V. Cabuil, *J. Nanopart. Res.* **11**, 459 (2008).
- [23] J. Cao, B. Wang, D. Han, S. Yang, J. Yang, M. Wei, L. Fan, Q. Liu, and T. Wang, *Cryst. Eng. Comm.* **15**, 6971 (2013).
- [24] Y. Fan, C. Ma, W. Li, and Y. Yin, *Mater. Sci. Semicond. Process.* **15**, 582 (2012).
- [25] L. Tan, X. Zhang, Q. Liu, X. Jing, J. Liu, D. Song, S. Hu, L. Liu, and J. Wang, *Colloids Surf. A* **469**, 279 (2015).
- [26] W. Stöber, A. Fink, and E. Bohn, *J. Colloid Interface Sci.* **26**, 62 (1968).
- [27] C. Li, R. Younesi, Y. Cai, Y. Zhu, M. Ma, and J. Zhu, *Appl. Catal. B Environ.* **156–157**, 314 (2014).
- [28] S. Liu, J. Yu, and S. Mann, *Nanotechnol* **20**, 325606 (2009).
- [29] T. D. Mitchell and L. C. De Jonghe, *J. Am. Ceram. Soc.* **78**, 199 (1995).
- [30] Y. Chi, Q. Yuan, Y. Li, L. Zhao, N. Li, X. Li, and W. Yan, *J. Hazard. Mater.* **262**, 404 (2013).
- [31] X. Yu, S. Liu, and J. Yu, *Appl. Catal. B Environ.* **104**, 12 (2011).
- [32] J. G. Yu, J. C. Yu, W. K. Ho, B. Cheng, X. J. Zhao, and J. C. Zhao, *J. Catal.* **217**, 69 (2003).
- [33] J. Yu, J. C. Yu, W. Ho, M. K. P. Leung, B. Cheng, G. Zhang, and X. Zhao, *Appl. Catal. A* **255**, 309 (2003).
- [34] J. Yu and B. Wang, *Appl. Catal. B Environ.* **94**, 295 (2010).
- [35] M. Zhou, J. Yu, S. Liu, P. Zhai, and B. Huang, *Appl. Catal. B Environ.* **89**, 160 (2009).
- [36] A. Enesca, M. Baneto, D. Perniu, L. Isac, C. Bogatu, and A. Duta, *Appl. Catal. B Environ.* **186**, 69 (2016).
- [37] V. C. Anitha, A. N. Banerjee, and S. W. Joo, *J. Mater. Sci.* **50**, 7495 (2015).
- [38] A. Hagfeldt and M. Graetzel, *Chem. Rev.* **95**, 49 (1995).
- [39] P. V. Kamat, *J. Phys. Chem. C* **112**, 18737 (2008).